Hydrogen-Transferred Radical Cations of NADH Model Compounds. 1. Spontaneous Tautomerization

Andrzej Marcinek,[†] Jan Adamus,[†] Krzysztof Huben,[†] Jerzy Gębicki,*,[†] Tadeusz J. Bartczak,[‡] Paweł Bednarek,[§,||] and Thomas Bally*,[||]

Contribution from the Institute of Applied Radiation Chemistry, Technical University, 90-924 Lodz, Poland, Institute of General and Ecological Chemistry, Technical University, 90-924 Lodz, Poland, Institute of Physical Chemistry, University of Fribourg, Perolles, CH-1700 Fribourg, Switzerland

Received January 28, 1999. Revised Manuscript Received November 4, 1999

Abstract: The radical cations generated from three NADH model compounds were investigated with particular emphasis on the possible formation of tautomeric enol radical cations. To a small extent, hydrogen transfer occurs upon ionization of all three compounds in argon matrixes. In the bicyclic seven-membered ring derivative enolization continues in a thermal reaction at 12 K (with highly dispersive kinetics), or upon visible irradiation. These processes are not observed in methylcyclohexane glasses at 77 K, which indicates that a cage effect is preventing the attainment of a reactive conformation in this medium. The assignment of electronic spectra of the primary (keto) cations and of their tautomeric (enol) forms is supported by CASSCF/CASPT2 and TD-B3LYP calculations.

1. Introduction

We have recently shown that certain classes of radical cations generated in cryogenic matrixes can undergo spontaneous tautomerization.[1,2] In many cases the neutral forms of these tautomers could be generated independently and characterized structurally. Spontaneous tautomerization in radical cations is a reaction of wide scope and it may also occur in cases in which the neutral enols cannot be observed.

In principle an approach of radical cation tautomerization can be expanded for radical cations generated from NADH model compounds. NADH radical cations can be viewed as reactive intermediates in NADH $\rightleftarrows$ NAD$^+$ conversion following a mechanism based on sequential electron−proton−electron transfer. Evidence to support the operation of such a mechanism in thermal, photochemical, and electrochemical oxidation of NADH and its analogues has been reported.[3−8] Also nonenzymatic transhydrogenation reactions involving NADH models seem to follow a sequential electron−proton−electron transfer mechanism.[9] These reactions are also important in the regeneration of NADH/NAD$^+$ coenzymes used extensively as chiral catalysts in asymmetric synthesis.[10]

Scheme 1

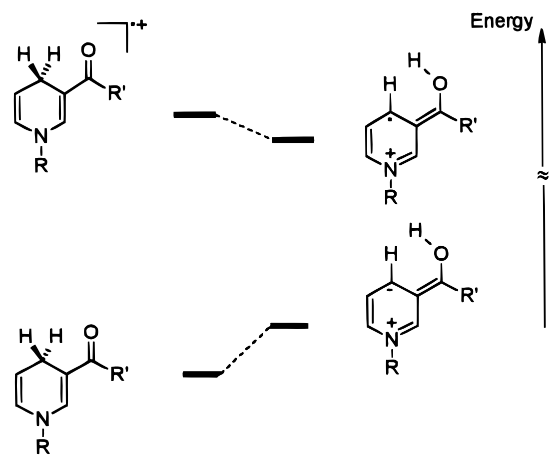

We recently attempted to apply a concept of radical cation tautomerization to nicotinamide derivatives (of which NADH is a member); however, we could find no spectroscopic evidence for the formation of tautomeric radical cations in cryogenic glasses, although AM1 calculations indicated enolization is exothermic in the radical cations, in contrast to the neutral species (see Scheme 1).[11] We concluded that, in NADH derivatives, where keto−enol tautomerization involves a 1,4-hydrogen atom shift, this process is associated with a relatively high activation barrier, and that it could proceed effectively only in radical cations which can assume a favorable geometry.

[†] Institute of Applied Radiation Chemistry.
[‡] Institute of General and Ecological Chemistry.
[§] On leave from the Institute of Applied Radiation Chemistry, Technical University, 90-924 Lodz, Poland.
[||] Institute of Physical Chemistry.

(1) Gębicki, J. *Pure Appl. Chem.* **1995**, *67*, 55.
(2) Gębicki, J.; Bally, T. *Acc. Chem. Res.* **1997**, *30*, 477.
(3) (a) Fukuzumi, S.; Tanaka, T. In *Photoinduced Electron Transfer*; Fox, M. A., Chanon, M., Eds.; Elsevier: Amsterdam, 1988; Part C, p 578. (b) Fukuzumi, S.; Suenobu, T.; Patz, M.; Hirasaka, T.; Itoh, S.; Fujitsuka, M. Ito, O. *J. Am. Chem. Soc.* **1998**, *120*, 8060.
(4) (a) Anne, A.; Fraoua, S.; Grass, V.; Moiroux, J.; Savéant, J.-M. *J. Am. Chem. Soc.* **1998**, *120*, 2951. (b) Anne, A.; Moiroux, J.; Savéant, J.-M. *J. Am. Chem. Soc.* **1993**, *115*, 10224. (c) Anne, A.; Hapiot, P.; Moiroux, J.; Neta, P.; Savéant, J.-M. *J. Am. Chem. Soc.* **1992**, *114*, 4694. (d) Anne, A.; Hapiot, P.; Moiroux, J.; Neta, P.; Savéant, J.-M. *J. Phys. Chem.* **1991**, *95*, 2370. (e) Hapiot, P.; Moiroux, J.; Savéant, J.-M. *J. Am. Chem. Soc.* **1990**, *112*, 1337.
(5) (a) Miller, L. L.; Valentine, J. R. *J. Am. Chem. Soc.* **1988**, *110*, 3982. (b) Carlson, B. W.; Miller, L. L. *J. Am. Chem. Soc.* **1985**, *107*, 479.
(6) Moiroux, J.; Elving, P. J. *J. Am. Chem. Soc.* **1980**, *102*, 6533.
(7) Almarsson, O.; Sinha, A.; Gopinath, E.; Bruice, T. C. *J. Am. Chem. Soc.* **1993**, *115*, 7093.
(8) Cheng, J.-P.; Lu, Y.; Zhu, X.; Mu, L. *J. Org. Chem.* **1998**, *63*, 6108.
(9) van Eikeren, P.; Kenny, P.; Tokmakian, R. *J. Am. Chem. Soc.* **1979**, *101*, 7402.
(10) Taylor, K. E.; Jones, J. B. *J. Am. Chem. Soc.* **1976**, *98*, 5689.
(11) Gębicki, J.; Marcinek, A.; Adamus, J.; Paneth, P.; Rogowski, J. *J. Am. Chem. Soc.* **1996**, *118*, 691.

10.1021/ja990286b CCC: $19.00 © 2000 American Chemical Society
Published on Web 01/06/2000

To establish the geometric requirements for enolization in radical cations of NADH models, we present here the results for two bicyclic derivatives, 1-methyl-1,4-dihydro-6,7,8,9-tetrahydro-5*H*-cyclohepta[b]pyridin-5-one (**1HK**) and 1-methyl-1,4,7,8-tetrahydro-5(6*H*)-quinolinone (**2HK**), and for the parent member of this series of compounds, 1-methyl-3-formyl-1,4-dihydropyridine (**3HK**).[12] The study of these compounds revealed that locking the carbonyl group in a *syn*-conformation with respect to C-4 carbon may not be sufficient to observe intramolecular tautomerization, but that a proper orientation of the CO group must also be secured. Also, it revealed that matrix effects may be quite important in determining the fate of the incipient radical cations derived from **1HK**−**3HK**. For the sake of simplicity we will denote the enol forms of the three compounds used in this study as **1HE**−**3HE**.[12]

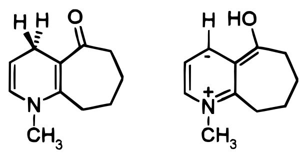

1HK **1HE**

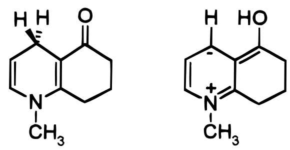

2HK **2HE**

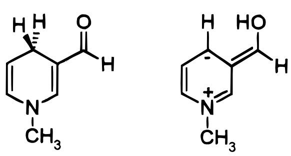

3HK **3HE**

2. Results and Discussion

2.1. Structural Properties and Energetics. The structures of **1HK** and **2HK** were determined by X-ray crystallography and by B3LYP/6-31G* density-functional calculations. In both compounds the six-membered pyridinium ring remains nearly planar, with only small deviations of the nitrogen and C-4 atoms from the mean atom plane. In contrast, the alicyclic side rings are considerably folded (see Figure 1), but this folding hardly affects the pyridine ring, which is only slightly more puckered in the seven-membered ring compound. However, it does change the critical orientation of the carbonyl group. This expresses itself clearly by the dihedral angle ω around the bond between the pyridine ring and the CO group which is only 1.9° in the crystal (1.1° in the isolated molecule by B3LYP) for **2HK**, whereas it is 7.5° (11.7°) for **1HK**.

This difference has repercussions on the distances between the O atom and the two hydrogen atoms on the C-4 carbon (see Table 1), although they remain in a similar range (2.55−2.77 Å) in both compounds. (They vary somewhat between the crystal structure and the calculation of the isolated molecule, which may indicate slight distortions induced by crystal packing forces.) More importantly, however, the structural change on

(12) The "**H**" is added to the symbols for the sake of consistency of the nomenclature with that of the second article[13] in which the corresponding neutral radicals and closed-shell cations that carry one hydrogen atom less are studied.

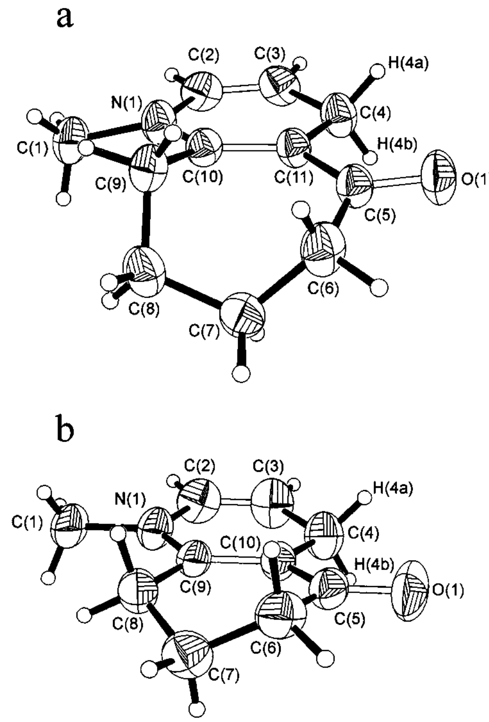

Figure 1. Side-on view of the crystallographic structures of **1HK** (a) and **2HK** (b). The thermal ellipsoids enclose 50% probability. Open sticks designate double bonds.

Table 1. Selected Crystallographic and Calculated Geometry Parameters of the Compounds Discussed in This Study[a]

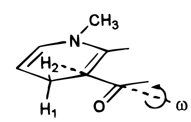

	ω	R(O···H$_1$)	R(O···H$_2$)
1HK (crystal)	7.5°	2.60 Å	2.64 Å
1HK (calc.)	11.7°	2.71 Å	2.55 Å
1HK$^{\bullet+}$ (calc.)	**25.9°**	**2.47 Å**	2.86 Å
2HK (crystal)	1.9°	2.56 Å	2.76 Å
2HK (calc.)	1.1°	2.64 Å	2.77 Å
2HK$^{\bullet+}$ (calc.)	2.0°	2.65 Å	2.68 Å
3HK (calc.)	0.0°	2.87 Å	2.87 Å
3HK$^{\bullet+}$ (calc.)	0.0°	2.78 Å	2.78 Å

[a] Full sets of Cartesian coordinates of all structures in this table are available in the Supporting Information.

ionization predicted by the calculations is very different in the two compounds: whereas ω changes by less than 1° in **2HK**, it increases by 14.2° in **1HK**! This results inter alia in a slight shortening of one of the two O···H distances to 2.47 Å, but it also changes the *orientation* of the carbonyl group relative to the prospective migrating C−H bond, which may be decisive if the in-plane p lone pair of the oxygen atom (n_O) acts as the acceptor of the migrating H atom. This is illustrated in more detail in Figure 2 which shows three different views on **1HK**$^{\bullet+}$ and **2HK**$^{\bullet+}$ as calculated by B3LYP/6-31G*.

From the above it becomes evident that in **1HK**$^{\bullet+}$ the n_O-molecular orbital (MO) is better aligned with the potentially migrating H-atom than in **2HK**$^{\bullet+}$ in every respect. Hence, **1HK** apparently would be a better candidate for spontaneous tautomerization on ionization than **2HK**. However, the distance across which this hydrogen atom transfer must take place is still considerable, so the strong distance dependence of this process[2,14] indicates that even **1HK**$^{\bullet+}$ may be a borderline case for spontaneous enolization.

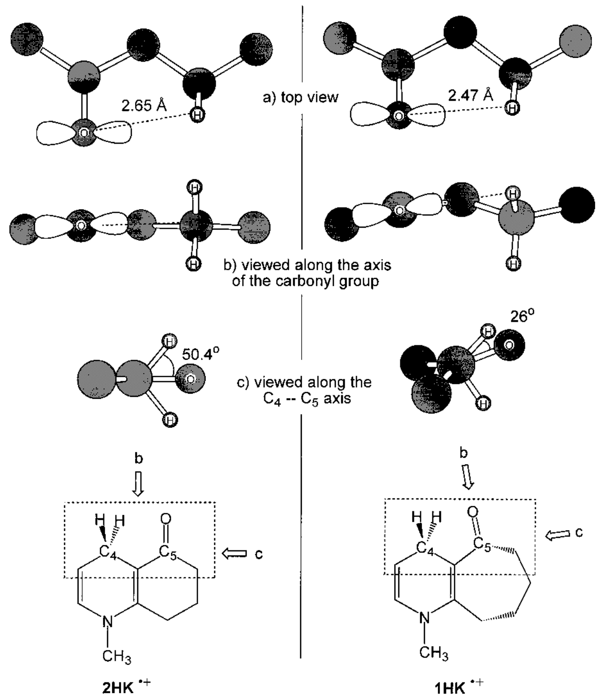

Figure 2. Different views of the B3LYP/6-31G* calculated structures of **2HK**$^{\bullet+}$ (left) and **1HK**$^{\bullet+}$ (right). Only the region boxed by the dashed line in the structural formulas is shown. The viewing positions b and c are indicated by open arrows. Note the alignment of the in-plane oxygen p-lone pair n_O with the hydrogen atom in **1HK**$^{\bullet+}$.

Table 2. Thermochemistry of Keto−Enol Tautomerization in NADH Model Compounds by B3LYP/6-31G* Calculations[a]

	ΔE (kcal/mol)
1HK→1HE	+32.8
1HK$^{\bullet+}$**→1HE**$^{\bullet+}$	−11.4
2HK→2HE	+35.7
2HK$^{\bullet+}$**→2HE**$^{\bullet+}$	−11.5
3HK→3HE	+35.4
3HK$^{\bullet+}$**→3HE**$^{\bullet+}$	−12.8

[a] All calculations at fully optimized geometries. Structures and total energies are given in the Supporting Information.

The B3LYP calculations above also yielded the energetics of the keto−enol tautomerization in the three 1,4-dihydropyridine derivatives (see Table 2), which is qualitatively in line with the earlier AM1 predictions.[11] Thus, enolization is endothermic by approximately 34 kcal/mol in the neutral compounds, whereas it becomes exothermic by about 12 kcal/mol in the radical cations. Apparently, the alkyl bridges have only a minor influence on the thermochemistry of this rearrangement in that ΔE is within 1−3 kcal/mol for all three compounds and their radical cations.

2.2. Matrix Isolation Experiments and Electronic Structure Calculations. 2.2.1. Keto Radical Cations. Ionization of the three model compounds embedded in argon matrixes leads to the electronic absorption (EA) spectra a−c in Figure 3. The most prominent feature of these spectra is a strong band located between 500 and 650 nm. Based on the experimental evidence presented in our preliminary study[11] we conclude that this band belongs to the parent (keto) radical cations of the three species. It shows distinct vibronic fine structure in **3HK**$^{\bullet+}$ (λ_{max} = 575 nm) and **2HK**$^{\bullet+}$ (λ_{max} = 608/592 nm), whereas this fine structure is blurred in the more flexible **1HK**$^{\bullet+}$ (λ_{max} = 575 nm).

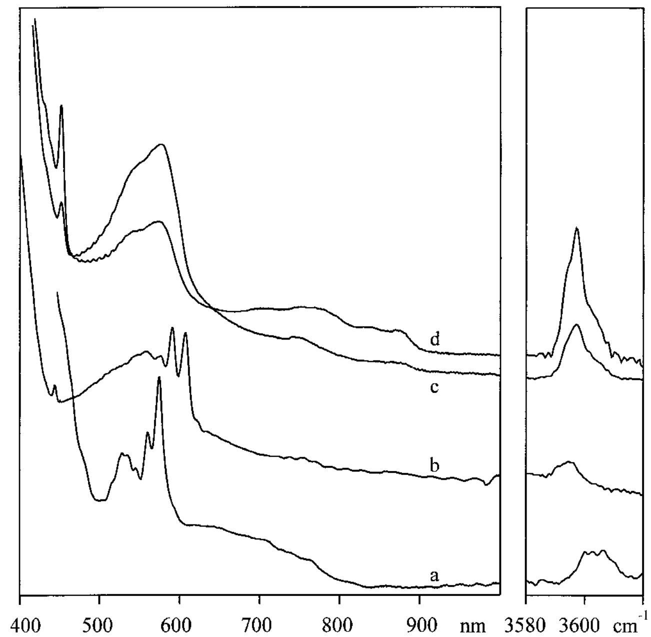

Figure 3. Electronic absorption and IR spectra obtained on ionization of **3HK** (a), **2HK** (b), and **1HK** (c) by X-irradiation of argon matrixes. Spectrum d shows the change of spectrum c on standing overnight at 12 K or on irradiation at 550 nm.

Table 3. Excited States of **3HK**$^{\bullet+}$ by CASPT2 Calculations

states	EAS, nm	CASPT2 nm	CASPT2 f^c	CASSCF configurations[a,b]
$1^2A''$	(0)	(0)	−	77% $(\pi_5)^1$ (ground state)
$1^2A'$	−	715	10^{-5}	80% $n_O \rightarrow \pi_5$
$2^2A''$	575	575	0.031	53% $\pi_4 \rightarrow \pi_5$
				22% $\pi_5 \rightarrow \pi_6^*$
$3^2A''$	<400	355	0.142	40% $\pi_5 \rightarrow \pi_6^*$
				29% $\pi_4 \rightarrow \pi_5$
$4^2A''$	−	285	0.003	25% $\pi_3 \rightarrow \pi_5$
				20% $\pi_5 \rightarrow \pi_7^*$ (+ others)

[a] Active space: 9 electrons in one occupied + one virtual a′ and 4 occupied + 4 virtual a″ MOs. [b] In terms of excitations within the manifold of MOs depicted in Figure 4. [c] Oscillator strength for electronic transition.

To confirm the above-mentioned assignment we carried out excited-state calculations by the CASSCF/CASPT2 method, which has given reliable predictions in closely related cases.[15] These calculations were limited to the parent compound, **3HK**$^{\bullet+}$ (see Table 3), for computational economy. Leaving aside the $n_O \rightarrow \pi_5$ excitation, which carries very little oscillator strength, they predict the first band of **3HK**$^{\bullet+}$ at 575 nm (2.38 eV), in excellent agreement with the 0−0 component of the intense visible band in spectrum a. Analysis of the CASSCF wave function shows that this excitation corresponds mainly to electron promotion from π_4 to the singly occupied MO (SOMO, π_5) mixed with some SOMO → lowest unoccupied molecular orbital (LUMO) excitation (for MOs, see Figure 4).

CASPT2 predicts a much more intense transition of **3HK**$^{\bullet+}$, which now corresponds predominantly to SOMO → LUMO electron promotion at 355 nm, but unfortunately this prediction cannot be verified because of strong absorptions of the neutral precursor. This is aggravated because X-irradiation of **3HK**

(13) Marcinek, A.; Rogowski, J.; Adamus, J.; Gębicki, J.; Bednarek, P.; Bally, T. *J. Phys. Chem.*, in press.
(14) Gębicki, J.; Marcinek, A.; Michalak, J.; Rogowski, J.; Bally, T.; Tang, W. *J. Mol. Struct.* **1992**, *275*, 249.
(15) Huben, K.; Zhu, Z.; Bally, T.; Gębicki, J. *J. Am. Chem. Soc.* **1997**, *119*, 2825.

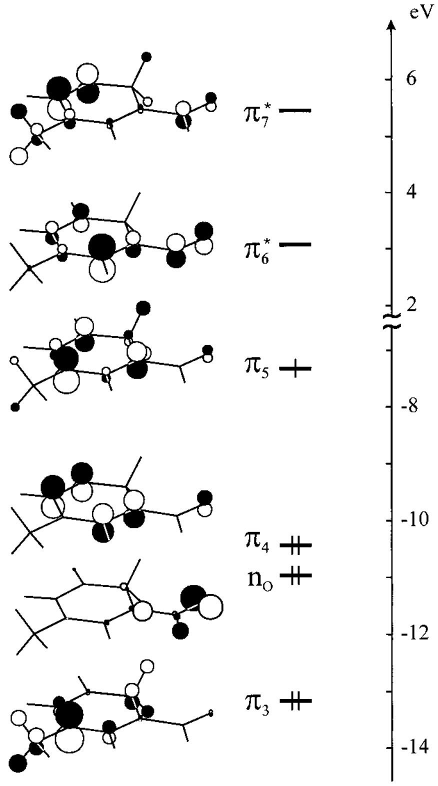

Figure 4. Molecular orbitals of **3HK** (at the radical cation geometry) involved in the excitations described in Table 3. Orbital energies are from SCF/6-31G* calculations of the neutral molecule.

Table 4. Lowest Excited States of Keto Radical Cations of NADH Model Compounds by TD-B3LYP Calculations

	1HK$^{•+}$		**2HK$^{•+}$**		**3HK$^{•+}$**		
states	nm	f^c	nm	f^c	nm	f^c	configurations[a,b]
$1^2A'$	989	~0	1181	~0	1063	~0	$n_O \rightarrow \pi_5$
$1^2A''$	520	0.046	520	0.045	485	0.036	$\pi_4 \rightarrow \pi_5$ $\pi_5 \rightarrow \pi_6^*$
$2^2A'$	383	~0	387	~0	383	~0	$n_O \rightarrow \pi_6^*$
$2^2A''$	356	0.063	347	0.074	346	0.107	$\pi_5 \rightarrow \pi_6^*$ $\pi_4/\pi_3 \rightarrow \pi_5$

[a] From the CIS-type output of the TD-DFRT calculation. [b] In terms of excitations within the manifold of MOs depicted in Figure 4. [c] Oscillator strength for electronic transition.

seems to induce also transformation to the less stable CHO anti-rotamer which absorbs at 450 nm.[16] However, the spectra of ionized **2HK** and **1HK** (3b and 3c, respectively) also show a strong rise toward the UV end of the spectra, which suggests the presence of an intense band of the cations below 400 nm, in agreement with the CASPT2 prediction for **3HK$^{•+}$**.

For **1HK$^{•+}$** and **2HK$^{•+}$**, for which we could not carry out CASPT2 calculations, we resorted to the much more economical time-dependent density functional response theory (TD-DFRT, see Experimental Section). This novel method has not been tested widely, so we also subjected **3HK$^{•+}$**, for which the results of the reliable CASPT2 calculations are available, to the TD-B3LYP procedure, the results of which are shown in Table 4. First, we should point out that the same excitations that dominated the lowest excited states in the CASSCF calculations (Table 3, last column) were found again in the TD-B3LYP calculations, so the results should be qualitatively comparable.

TD-B3LYP places the $n_O \rightarrow \pi_5$ excited state of **3HK$^{•+}$** at 0.55 eV lower energy than CASPT2, a prediction that we cannot

(16) Gębicki, J.; Bednarek, P.; Bally, T., manuscript to be published.

Table 5. Excited States of **3HE$^{•+}$** by CASPT2 Calculations

		CASPT2		
states	EAS, nm	nm	f^c	CASSCF configurations[a,b]
$1^2A''$	(0)	(0)	–	84% $(\pi_6)^1$ (ground state)
$2^2A''$	≈750	720	0.018	75% $\pi_6 \rightarrow \pi_7^*$
$3^2A''$	<450	435	0.006	39% $\pi_6 \rightarrow \pi_8^*$ 34% $\pi_5 \rightarrow \pi_6$
$4^2A''$	–	295	0.008	34% $\pi_5 \rightarrow \pi_6$ 10% $\pi_5 \rightarrow \pi_7^*$ (+ others)

[a] Active space: 11 electrons in 2 occupied a′ and 5 occupied + 4 virtual a″ MOs. [b] In terms of excitations within the manifold of MOs depicted in Figure 5. [c] Oscillator strength for electronic transition.

verify experimentally. In contrast, the first π-excited ($^2A''$) state of **3HK$^{•+}$** is predicted 0.4 eV higher than by CASPT2 and/or experiment, but TD-B3LYP predicts a red shift on going to both cyclic compounds, in accord with experiment. Owing to the distinct vibronic structure of its absorption band, this shift is seen more clearly for **2HK$^{•+}$**. After another $n_O \rightarrow \pi$ excitation with almost no oscillator strength (which were missed in the CASPT2 calculations above), the next π-excited state is predicted in excellent accord with CASPT2.

2.2.2. Enol Radical Cations. Returning to the spectra in Figure 3 we note the presence of a *second species* with a weak, broad band at 700−900 nm and a sharp peak around 450 nm. In ionized **2HK** and **3HK**, the visible range of the spectra remains unchanged on annealing of the matrix to 25 K or on irradiation at various wavelengths (in **3HK** the 450 nm absorption of the minor rotamer gains intensity on UV photolysis[16]). In contrast, overnight standing of **1HK$^{•+}$** at 12 K, or photolysis at 550 nm, converts spectrum 3c to 3d, i.e., the 700−900 nm band system and the 450 nm peak increase significantly in intensity at the expense of the strong 575 nm band of **1HK$^{•+}$**. At the same time a conspicuous band at 3600 cm^{-1} in the IR spectrum doubles in intensity (see Figure 3, right-hand side), along with some of the other IR bands which had arisen during X irradiation.[17] This 3600 cm^{-1} band is typical of enol radical cations[14,18] and thus indicates that the observed process corresponds to enolization of **1HK$^{•+}$**. A similar IR band is also present after ionization of **2HK** and **3HK**, but it is weaker than in ionized **1HK**, which indicates a more facile enolization of the latter compound.

The CASPT2 calculations listed in Table 5 support the assignment of these spectral features to enol radical cations. Whereas the predicted weak first transition of **3HE$^{•+}$** can be discerned as a double-humped band at 765/710 nm in spectrum 3a, the sharp blue peak is once again obscured by the absorptions of neutral **3HK**. However, its clear identification in the spectra of **2HE$^{•+}$** (λ_{max} = 443 nm) leaves little doubt that a similar band is to be expected also in **3HE$^{•+}$**, probably with a small blue shift, which would bring it into the vicinity of the predicted position (cf. also the TD-B3LYP results presented below). From the CASSCF wave functions we gather that the weak red band corresponds essentially to SOMO → LUMO excitation (for MOs see Figure 5), whereas the excited state corresponding to the UV band arises by a mixture of $\pi_6 \rightarrow \pi_8$* and $\pi_5 \rightarrow \pi_6$ electron promotions.

Again, we resorted to TD-B3LYP calculations for the related enol radical cations, **1HE$^{•+}$** and **2HE$^{•+}$** (see Table 6). This time the agreement with CASPT2 (and experiment) is much better for the first π excited state, and the ≈100 nm blue shift on

(17) Unfortunately, the C═O stretching band of the keto radical cation cannot be monitored easily because of overlapping neutral absorptions.

(18) Marcinek, A.; Michalak, J.; Rogowski, J.; Tang, W.; Bally, T.; Gębicki, J. *J. Chem. Soc., Perkin Trans. 2* **1992**, 1353.

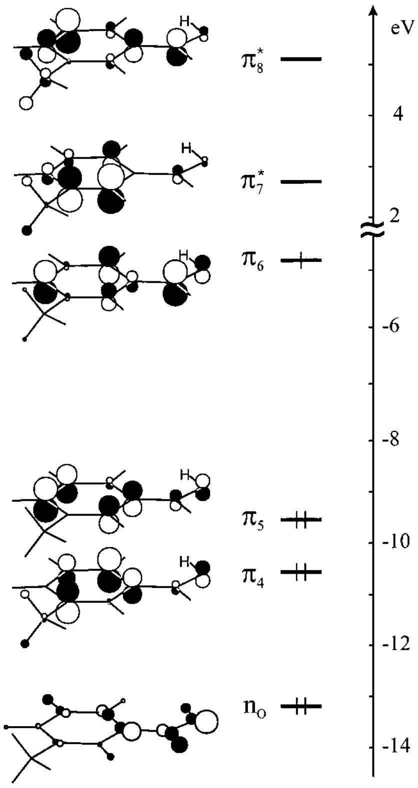

Figure 5. Molecular orbitals of **3HE** (at the radical cation geometry) involved in the excitations described in Table 5. Orbital energies are from SCF/6-31G* calculations of **3HE**.

Table 6. Lowest Excited States of Enol Radical Cations of NADH Model Compounds by TD-B3LYP Calculations

	$1HE^{•+}$		$2HE^{•+}$		$3HE^{•+}$		
states	nm	f^c	nm	f^c	nm	f^c	configurations[a,b]
$2^2A''$	831	0.008	790	0.009	727	0.009	$\pi_6 \rightarrow \pi_7^*$
$3^2A''$	400	0.065	380	0.056	370	0.048	$\pi_6 \rightarrow \pi_8^*$
							$\pi_5 \rightarrow \pi_6$
$4^2A''$	307	0.016	301	0.016	294	0.017	$\pi_4/\pi_5 \rightarrow \pi_7^*$

[a] From the CIS-type output of the TD-DFRT calculation. [b] In terms of excitations within the manifold of MOs depicted in Figure 5. [c] Oscillator strength for electronic transition.

going from $1HE^{•+}$ to $3HE^{•+}$ ($\lambda_{max} = 875/775$ nm for the first band) is also predicted correctly. (This weak band cannot be observed clearly in $2HE^{•+}$.) The second excited state which gives rise to the sharp 453 nm band in $1HE^{•+}$ is 0.35 eV too high in energy, but TD-B3LYP predicts a $\approx$30 nm blue shift of this band on going from $1HE^{•+}$ to $3HE^{•+}$. This places the second absorption of $3HE^{•+}$ into the region that is obscured by the absorptions of neutral **3HK**. No other excited states are predicted to lie in the observable region for either of the enol cations.

Observing the kinetics of the slow thermal enolization of $1HK^{•+}$ in Ar at 12 K gave the kinetic traces shown in Figure 6, which indicate clearly that the process follows dispersive rather than classical kinetics. If analyzed in terms of dispersive kinetics with the rate constant depending on time in the form: $k(t) = B{\cdot}t^{\alpha-1}$,[19,20] a mean lifetime of $\tau = 140$ h and a dispersion parameter $\alpha = 0.5$ were found for this process. (Kinetic curves obtained with these parameters are shown as solid lines in Figure 6.) This value of α is characteristic for hydrogen atom transfer processes in matrixes and was often applied in analyses of such reactions.[21−24] It indicates that different matrix sites offer different amounts of resistance to the attainment of an optimal conformation for tautomerization. It cannot be excluded that the thermal process involves a contribution from hydrogen atom tunneling as it was observed in enolization of radical cations of aryl ketones.[14,18]

(19) Płonka, A. *Annu. Rep. Prog. Chem.* **1989**, *85*, 47.
(20) Compare: Marcinek, A.; Gębicki, J.; Płonka, A. *J. Phys. Org. Chem.* **1990**, *3*, 757.

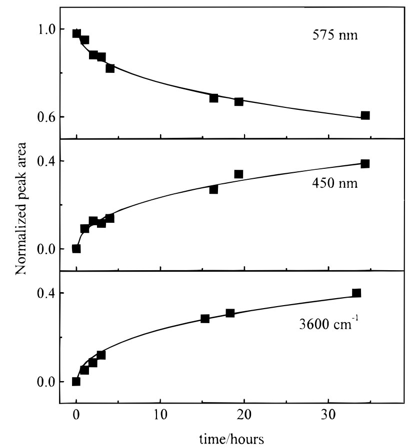

Figure 6. Decay of $1HK^{•+}$ (575 nm band) and growth of $1HE^{•+}$ (450 nm and 3600 cm^{-1} bands). Solid lines represent the fitting of dispersive kinetics ($\alpha = 0.5$) to the experimental points (discussion, see text).

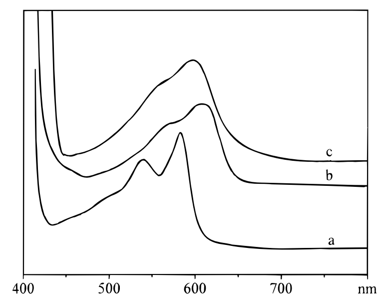

Figure 7. Electronic absorption spectra obtained on electron impact ionization of **3HK** (a) in 2-chlorobutane, **2HK** (b), and **1HK** (c) in methylcyclohexane/2-chlorobutane (3:1) at 77 K (**3HK**: $1{\cdot}10^{-2}$ M solution, radiation dose 10 kGy, sample thickness 3 mm; **2HK**: $2{\cdot}10^{-2}$ M solution, radiation dose 7 kGy, sample thickness 2 mm; **1HK**: saturated solution, radiation dose 8 kGy, sample thickness 3 mm).

We also carried out ionizations in methylcyclohexane/2-chlorobutane (MCH/BuCl) glasses at 77 K. In view of the observed thermal enolization of $1HK^{•+}$ at 12 K in Ar, one would have expected to see very little, if any, $1HK^{•+}$ (and possibly $2HK^{•+}$) in MCH/BuCl. The optical spectra obtained after electron impact ionization of **1HK**, **2HK**, and **3HK**, respectively (see Figure 7), however, showed no trace of the sharp UV bands around 450 nm which are indicative of the enol cations. To some extent the enolization process can be driven by an excess energy released in the ionization process. This is much higher if ionization occurs by hole transfer from $Ar^{•+}$, and the comparatively small amount that is available on ionization in MCH is dissipated much more readily in this solvent and hence is not available to drive activated processes.

The absence of thermal and/or the photochemical enolization of $1HK^{•+}$ at 77 K is more difficult to explain. Perhaps the MCH/

(21) Siebrand, M.; Wildman, T. A. *Acc. Chem. Res.* **1986**, *19*, 238.
(22) Platz, M. S. *Acc. Chem. Res.* **1988**, *21*, 236.
(23) McMahon, R. J.; Chapman, O. L. *J. Am. Chem. Soc.* **1985**, *107*, 683.
(24) Admasu, A.; Platz, M. S.; Marcinek, A.; Michalak, J.; Gudmundsdottir, A. D.; Gębicki, J. *J. Phys. Org. Chem.* **1997**, *10*, 207.

BuCl matrix prevents **1HK**$^{•+}$ from undergoing full relaxation to its equilibrium conformation where the n_O p-MO is oriented toward the migrating H-atom (cf. Figure 2). An indication that this might be the case is the 20 nm red shift in λ_{max} of the visible band in **1HK**$^{•+}$ on going from argon to MCH/BuCl, especially because this shift is much smaller in **2HK**$^{•+}$ where ionization involves no comparable conformational changes. The calculated energy for the relaxation of **1HK**$^{•+}$ from the neutral geometry is only 3.7 kcal/mol, which indicates that the potential energy surface for this process is very flat, and hence susceptible to distortion by cage effects. If **1HK**$^{•+}$ is prevented from attaining its equilibrium conformation, the activation barrier for H-transfer may be raised sufficiently to prohibit enolization of **1HK**$^{•+}$, even at 77 K.

Two explanations are possible regarding the nonoccurrence of the photochemical enolization: either internal conversion to the ground state is more efficient in the polyatomic solvent matrix, which may prevent a crossover from the excited state of **1HK**$^{•+}$ to the ground-state surface of **1HE**$^{•+}$, or the reaction proceeds as a thermal process caused by local heating and softening of the matrix, which may be more effective in Ar than in MCH/BuCl.

3. Conclusions

In this article we present the first direct experimental evidence for intramolecular hydrogen atom transfer upon ionization of NADH model compounds. The optical spectra of the keto and enol forms of the radical cations are assigned with the help of CASSCF/CASPT2 and TD-DFRT calculations. Although the predictions from the latter method are not as accurate as from the former, they result in a qualitatively correct picture of the electronic structure of the species observed in this study.

Only one of the model compounds used in this study (**1HK**) seems particularly well disposed for spontaneous tautomerization of the radical cation, in that the reaction proceeds slowly even at 12 K in argon matrixes (and, more quickly, on photolysis at 550 nm). B3LYP calculations indicate that on ionization **1HK** distorts to a structure in which the in-plane oxygen lone pair is almost perfectly aligned for accepting the migrating H-atom, in contrast to the other compounds that remain nearly planar on ionization. This distortion of **1HK**$^{•+}$ also reduces the distance for the H-transfer by about 0.15 Å, although this still remains rather large (2.47 Å). Thus, **1HK**$^{•+}$ represents a borderline case for spontaneous tautomerization on ionization of NADH model compounds. The structure of this radical cation mimics to some extent the *syn*-conformation (with the amide group rotated 20−30° out of plane) of dihydronicotinamide moiety of NADH observed in most of the enzymatically active sites.[25−27]

In a second article[13] we will show that radical cations of the type **HE**$^{•+}$ can also be formed by sequential electron−proton addition to NAD^+ model compounds. This approach will prove to be more general because no special geometric requirements are needed for the formation of enol radical cations.

3. Experimental Section

3.1. Syntheses. 3.1.1. 1-Methyl-1,4-dihydro-6,7,8,9-tetrahydro-5*H*-cyclohepta[b]pyridin-5-one (1HK). The procedure of Epsztajn et al.[28] was followed to prepare [2,3]cycloheptenopyridine. This was further oxidized to 6,7,8,9-tetrahydro-5*H*-cyclohepta-[b]pyridin-5-one (yield 5%) by a mixture of CrO_3 and H_2SO_4 according to the described procedure.[29] A solution of the tetrahydrocycloheptapyridinone (0.85 g; 5.3 mmol) and methyl iodide (1.5 g; 10.5 mmol) in 10 mL of ethyl ether was kept at room temperature for 48 h to give 1.4 g (87%) of 1-methyl-6,7,8,9-tetrahydro-5*H*-cyclohepta[b]pyridinium-(5-one) iodide, mp 218−219 °C. [The salt was converted to chloride (**1**$^+$) by shaking its water solution with freshly precipitated silver chloride.] To a stirred, degassed solution of iodide salt (0.5 g; 1.7 mmol) and $NaHCO_3$ (0.5 g; 6 mmol) in 10 mL of water, sodium dithionite (1 g; 5.5 mmol) and 1 g of NaCl were added during a 15-min period. The precipitated product was filtered off, dried over P_2O_3 in vacuo, purified by column chromatography, and crystallized from degassed methylcyclohexane at −15 °C to give 0.18 g (60%) of 1-methyl-1,4-dihydro-6,7,8,9-tetrahydro-5*H*-cyclohepta[b]pyridin-5-one (**1HK**), mp 107−108 °C. ^1H NMR (200 MHz, $CDCl_3$ δ ppm: 1.77 (m, 4H, $2CH_2$), 2.60 (m, 4H, $2CH_2$), 3.03 (d, 2H, CH_2), 3.06 (s, 3H, CH_3), 4.87 (m, 1H), 5.69 (m, 1H).

3.1.2. 1-Methyl-1,4,7,8-tetrahydro-5(6*H*)-quinolinone (2HK). Freshly obtained propiolaldehyde[30] (8.2 g; 152 mmol) was added[31] dropwise to a solution of 1-aminocyclohexane-3-one (8.4 g; 76 mmol; obtained by reacting cyclohexanedione-1,3 with ammonia) in 220 mL of dimethylformamide (DMF). The solution was stirred at room temperature for 18 h, then the solvent was evaporated in vacuo and the residue was distilled (116−118 °C, 6 mmHg) to give 6.4 g (58%) of 7,8-dihydro-5(6*H*)-quinolinone. A solution of the dihydroquinolinone (5 g; 34 mmol) and methyl iodide (10 g; 70.4 mmol) in 70 mL of diethyl ether was kept at room temperature for 24 h to give 8.3 g (84%) of 1-methyl-7,8-dihydro-5(6*H*)quinolinonium iodide (**2**$^+$), mp 241−242 °C. To a stirred, degassed solution of **2**$^+$ (1 g; 3.5 mmol) and $NaHCO_3$ (0.8 g; 9.5 mmol) in 17 mL of water, sodium dithionite (2 g; 11 mmol) was added during a 10-min period. Then 3 g of NaCl was added and after an additional 5 min the precipitated product was filtered off, washed with cold water (5 mL), and vacuum-dried over P_2O_3. The crude product was purified by column chromatography and then crystallized from degassed methylcyclohexane at −10 °C to give 0.31 g (54%) of 1-methyl-1,4,7,8-tetrahydro-5(6*H*)-quinolinone (**2HK**), mp 112−113 °C. ^1H NMR (200 MHz, $CDCl_3$) δ ppm: 1.97 (m, 2H, CH_3), 2.37 (m, 4H, $2CH_2$), 3.01 (s, 3H, CH_3), 3.05 (d, 2H, CH_2), 4.89 (m, 1H), 5.69 (m, 1H).

3.1.3. 1-Methyl-3-formyl-1,4-dihydropyridine (3HK). A solution of freshly distilled 3-formylpyridine (Aldrich, 6 g, 56 mmol) and CH_3I (11 g, 80 mmol) in 50 mL of dry ethyl ether was kept overnight at room temperature. The precipitated salt was filtered off, washed with ether, and crystallized from anhydrous acetone to give 11.8 g (85%) of 1-methyl-3-formylpyridinium iodide. The salt was then converted to chloride (**3**$^+$) by shaking its water solution with freshly precipitated silver chloride (mp 188−190 °C). To a stirred, degassed solution of sodium dithionite (5 g) and sodium carbonate (1.4 g) in 30 mL of water, 2 g (8 mmol) of **3**$^+$ as chloride salt was added during a 10-min period. The resulting solution was extracted with CH_2Cl_2 overnight. The solvent was removed under vacuum and the residual oil was pumped out and dried over P_2O_5 to give very hygroscopic crystals. ^1H NMR (80 MHz, $CDCl_3$) δ ppm: 3.04 (s, 3H, CH_3), 3.09 (s, 2H, CH_2), 4.92 (m, 1H), 5.78 (m 1H), 6.61 (s, 1H), 9.08 (s, 1H, C(O)H).

3.2. X-ray Crystallography. 1HK was crystallized from methylcyclohexane in space group $P2_12_12_1$ with $a = 7.447(1)$, $b = 8.993(2)$, $c = 13.818(2)$ Å, $V = 925.40(18)$ Å^3, and $Z = 4$. Data were collected at room temperature on a KUMA-4 diffractometer with Cu$K\alpha$ radiation. A total of 2626 reflections ($-1 \le h \le 9$, $-1 \le k \le 10$, $-17 \le l \le 17$, max $2\theta = 162.30°$) were recorded with 1844 of them unique. The structure was solved with SHELXS97 and refined with SHELXL97[32] using full-matrix−least-squares technique on F_o^2 to $R1 = 0.048$ for

(25) Oppenheimer, N. J.; Handlon, A. L. In *The Enzymes*; Sigman, D. S., Ed.; Academic Press: San Diego, 1992; p 453.
(26) Wu, Y.-D.; Houk, K. N. *J. Org. Chem.* **1993**, *58*, 2043.
(27) Brewster, M. E.; Pop, E.; Huang, M.-J.; Bodor, N. *Heterocycles* **1994**, *37*, 1373.
(28) Epsztajn, J.; Bienek, A.; Brzezinski, J. Z. *Pol. J. Chem.* **1980**, *54*, 341.
(29) Bradley, W. C.; Jaen, J. C.; Wise, L. D.; Heffner, T. G.; Pugsley, T. A.; Meltzer, L. T.; Parvez, M. *J. Med. Chem.* **1991**, *34*, 2736.
(30) Wilde, F.; Saffer, L. *Liebigs Ann. Chem.* **1950**, *568*, 34.
(31) Zymalkowski, F.; Rimek, H. *Arch. Pharm., Weinheim, Ger.* **1961**, *294*, 759.
(32) Sheldrick, G. M. *SHELXS/SHELXL: A Set of Programs to Solve and Refine Crystal Structures*, Version 97; University of Göttingen: Germany, 1997.

1494 $F_o > 4\sigma(F_o)$, and $R1 = 0.063$ and $wR2 = 0.130$ for all 1843 data; goodness of fit $s = 0.973$. All hydrogen atoms were found from difference Fourier syntheses and were refined as "riding" on their parent carbon atoms.

2HK was crystallized from methylcyclohexane in space group *Pcnn* with $a = 10.133(1)$, $b = 10.291(1)$, $c = 16.475(2)$ Å, $V = 1717.99(23)$ Å^3, and $Z = 8$. A needlelike crystal (0.08 × 0.08 × 0.83 mm) was used for the data collection on a KUMA-4 single-crystal diffractometer with Cu$K\alpha$ ($\lambda = 1.54178$ Å) radiation at room temperature. A total of 2078 reflections were recorded ($0 \le h \le 10$, $0 \le k \le 13$, $-1 \le l \le 18$, max $2\theta = 161.38°$) to give 1675 unique reflections. The structure was solved and refined as above (F_o^2 to $R1 = 0.041$ for 904 $F_o > 4\sigma(F_o)$, and $R1 = 0.106$ and $wR2 = 0.131$ for all 1675 data; goodness of fit $s = 0.973$).

The data for both crystal structures have been deposited at the Cambridge Crystallographic Data Center and were allocated the numbers CCDC104486 (**2HK**) and CCDC104487 (**1HK**). Crystal structures in Cartesian coordinates are included in the Supporting Information.

3.3. Matrix Isolation and Spectroscopy. Crystals of the compounds were placed in a U-shaped tube immersed in a water bath and connected to the inlet system of a closed-cycle cryostat. While the bath was kept at 25, 60, or 70 °C for **3HK**, **2HK,** and **1HK**, respectively, a mixture of argon and methylene chloride flowed through the tube at a rate of ≈1 mmol/h and swept the compounds onto a CsI window held at 19 K. There the mixture accumulated to form a matrix containing a sufficient quantity of the compound within 2 h.

After taking reference spectra, the samples were exposed to 90 min of X-irradiation as described previously.[33] Photolyses were effected with a 1-kW Ar plasma discharge lamp through a 550 nm interference filter. EA spectra were taken between 200 and 1200 nm with a Perkin-Elmer Lambda 19 instrument, whereas IR spectra were obtained on a Bomem DA3 interferometer (1 cm^{-1} resolution) equipped with an MCT detector (500−4000 cm^{-1}).

A description of the pulse radiolysis system and methodology of the low-temperature studies in organic matrixes are given elsewhere.[34,35]

3.4. Quantum Chemical Calculations. The geometries of all species were optimized by the B3LYP density-functional method[36,37] as implemented in the Gaussian 94 suite of programs,[38,39] using the 6-31G* basis set. Relative energies were calculated at the same level. Full sets of Cartesian coordinates and absolute energies (including thermal corrections where available) are given in the Supporting Information.

Excited-state calculations on **3HK**$^{\bullet+}$ and **3HE**$^{\bullet+}$ were carried out at the B3LYP/6-31G* geometries of the radical cations by the CASSCF/CASPT2 procedure[40] with the MOLCAS program[41] using the [C,N,O]-3s2p1d/[H]2s ANO basis set.[42] The active spaces were chosen to obtain a satisfactory description of the excited states of interest at the CASPT2 level. (The CASPT2 wave functions are described to 68−72% by the CASSCF wave function for all excited states except the $3^2A''$ state of the enol radical cation where, because of an intruder state, it is only 61%.) This resulted in a (9,10) active space for **3HK**$^{\bullet+}$ and a (11,11) active space for **3HE**$^{\bullet+}$. (The active spaces are described in detail in the footnotes to Tables 3 and 5.) To ensure orthogonality, the CASSCF wave functions were averaged over all the excited states of interest. Transition moments were calculated on the basis of these wave functions, using CASPT2 energy differences in the denominator.

For the bicyclic derivatives **1H** and **2H** we resorted to a recently introduced molecular density-functional method based on time-dependent response (TDR) theory.[43] Analogous to the Hartree−Fock TDR theory (e.g., in the Tamm−Dancoff or Random-Phase approximation), the poles and the residues of the frequency-dependent polarizability are evaluated, where the former correspond to vertical excitation energies and the latter to oscillator strengths. Also analogous to HF-TDR, excited states are then described in terms of CI vectors containing single excitations from a ground state wave function (CIS), which permits a very transparent interpretation of the results. However, the treatment of electron correlation in TD-DFRT goes far beyond that in a HF-based CIS method, which means that the results are generally more accurate. We used the implementation of TD-DFRT described recently by Stratmann et al.[44] and implemented in the Gaussian 98 program,[45] together with the B3LYP functional. To our best knowledge, we present the first application of this model to open-shell systems.

Acknowledgment. This work was supported by grants from the State Committee for Scientific Research (No. 3/*T*09A/097/11) and the Swiss National Science Foundation (No. 2000-053568.98). We thank Markus Fülscher (University of Lund, Sweden) for help with the CASPT2 calculations. J.G. thanks Foundation on behalf of Polish Science for support within the program "Subsidies for Scholars".

Supporting Information Available: Listing of Cartesian coordinates of crystal structures for **1HK** and **2HK** as well as energies and Cartesian coordinates from the B3LYP calculations for all compounds mentioned in this study (neutrals and radical cations) are available in ASCII format. This material is available free of charge via the Internet at http://pubs.acs.org.

JA990286B

(33) Bally, T. In *Radical Ionic Systems*; Lund, A., Shiotani, M., Eds.; Kluwer: Dordrecht, 1991; p 3.

(34) Karolczak, S.; Hodyr, K.; Łubis, R.; Kroh, J. *J. Radioanal. Nucl. Chem.* **1986**, *101*, 177.

(35) Gębicki, J.; Marcinek, A.; Rogowski, J. *J. Radiat. Phys. Chem.* **1992**, *39*, 41.

(36) Becke, A. D. *J. Chem. Phys.* **1993**, *98*, 5648.

(37) Lee, C.; Yang, W.; Parr, R. G. *Phys. Rev. B* **1988**, *37*, 785.

(38) Frisch, M. J.; Trucks, G. W.; Schlegel, H. B.; Gill, P. M. W.; Johnson, B. G.; Robb, M. A.; Cheeseman, J. R.; Keith, T.; Petersson, G. A.; Montogomery, J. A.; Raghavachari, K.; Al-Laham, M. A.; Zakrzewski, V. G.; Ortiz, J. V.; Foresman, J. B.; Cioslowski, J.; Stefanov, B. B.; Nanayakkara, A.; Challacombe, M.; Peng, C. Y.; Ayala, P. Y.; Chen, W.; Wong, M. W.; Andres, J. L.; Repogle, E. S.; Gomperts, R.; Martin, R. L.; Fox, D. J.; Binkley, J. S.; DeFrees, D. J.; Baker, J.; Stewart, J. P.; Head-Gordon, M.; Gonzales, M. C.; Pople, J. A. *Gaussian 94*, Rev. B1 and D4; Gaussian, Inc.: Pittsburgh, PA, 1995.

(39) For a description of the DFT methods implemented in the Gaussian program, see Johnson, B. G.; Gill, P. M. W.; Pople, J. A. *J. Chem. Phys.* **1993**, *98*, 5612.

(40) Andersson, K.; Roos, B. O. In *Modern Electronic Structure Theory*; World Scientific Publ. Co.: Singapore, 1995; Part 1, Vol. 2, p 55.

(41) Andersson, K.; Blomberg, M. R. A.; Fülscher, M. P.; Kellö, V.; Lindh, R.; Malmqvist, P.-Å.; Noga, J.; Olson, J.; Roos, B. O.; Sadlej, A.; Siegbahn, P. E. M.; Urban, M.; Widmark, P.-O. *MOLCAS*, Versions 3 and 4; University of Lund: Sweden, 1994.

(42) Pierloot, K.; Dumez, B.; Widmark, P.-O.; Roos, B. O. *Theor. Chim. Acta* **1995**, *90*, 87.

(43) Casida, M. E. In *Recent Advances in Density Functional Methods, part I*; Chong, D. P., Ed.; World Scientific: Singapore, 1995; p 155.

(44) Stratmann, R. E.; Scuseria, G. E.; Frisch, M. J. *J. Chem. Phys.* **1998**, *109*, 8218.

(45) Frisch, M. J.; Trucks, G. W.; Schlegel, H. B.; Scuseria, G. E.; Robb, M. A.; Cheeseman, J. R.; Zakrzewski, V. G.; Montgomery, J. A.; Stratmann, R. E.; Burant, J. C.; Dapprich, S.; Millam, J. M.; Daniels, A. D.; Kudin, K. N.; Strain, M. C.; Farkas, O.; Tomasi, J.; Barone, V.; Cossi, M.; Cammi, R.; Mennucci, B.; Pommelli, C.; Adamo, C.; Clifford, S.; Ochterski, J.; Petersson, G. A.; Ayala, P. Y.; Cui, Q.; Morokuma, K.; Malick, D. K.; Rabuck, A. D.; Raghavachari, K.; Foresman, J. B.; Cioslowski, J.; Ortiz, J. V.; Stefanov, B. B.; Liu, G.; Liashenko, A.; Piskorz, P.; Komaromi, I.; Gomperts, R.; Martin, R. L.; Fox, D. J.; Keith, T.; Al-Laham, M. A.; Peng, C. Y.; Nanayakkara, A.; Challacombe, M.; Gill, P. M. W.; Johnson, B. G.; Chen, W.; Wong, M. W.; Andres, J. L.; Gonzales, C.; Head-Gordon, M.; Repogle, E. S.; Pople, J. A. *Gaussian 98*, Rev. A1; Gaussian, Inc.: Pittsburgh, PA, 1998.